

## MEASUREMENT OF DOWNWASH VELOCITY GENERATED BY ROTORS OF AGRICULTURE DRONES

### 植保无人机旋翼下洗气流速度的测量

As. Prof. Ph.D. Tan Feng<sup>\*1)</sup>, Ph.D. Lian Qi<sup>2)</sup>, M.S. Liu Chang-liang<sup>3)</sup>, M.S. Jin Bing-kun<sup>4)</sup>

<sup>1)</sup> School of Electrical and Information, Heilongjiang Bayi Agricultural University, Daqing / China; <sup>2)</sup> School of Engineering, Heilongjiang Bayi Agricultural University, Daqing / China; <sup>3)</sup> Key Laboratory of Surface Engineering of Equipment for Hydraulic Engineering of Zhejiang Province, Hangzhou / China; <sup>4)</sup> Faculty of Mechanical and Materials Engineer, Western University, London/Canada  
Tel: +8613836962600; E-mail: tf1972@163.com

**Keywords:** agriculture drone; downwash velocity; rotors; measurement

#### ABSTRACT

With the rapid development of drones in China, the use of multi-rotor drones for spraying chemical pesticide against pests and weeds has recently become common in agriculture. However, the downwash generated by drone rotors considerably influences the droplet deposition process by potentially causing the liquid to drift. A test analysis method was presented and a rotor rotation test bench was designed to simulate the different rotation speed of a six-rotor drone and thus study the characteristics and distribution law of the downwash velocity. An anemometer was used to measure the downwash velocity generated at different radial positions of the rotor. Results show that the downwash velocity generated by each radial position of the rotor is evenly distributed on the rotating loop and the standard deviation of the circumferential downwash velocity is less than 1 m/s. The downwash velocity along each position in the radial direction of the rotor increase first and then decrease and the 1/2 radius position of rotor blade generate the maximum downwash velocity of 10.8 m/s in the test. The downwash velocity does not considerably change with longitude, but decreases at a distance of 10 cm from the ground due to the ground effect. Therefore, the parameters of airfoil profile at each radial position on the rotors have a marked effect on the magnitude of the downwash velocity. This study provides an effective measurement method for the investigation of the downwash velocity distribution of drone rotors. The measurement results can provide a reference for the nozzle distribution under the rotor and the study of droplet movement.

#### 摘要

随着无人机在中国的快速发展,近年来在农业领域使用多旋翼无人机喷洒化学药剂进行病虫害防治变得越加普遍。但由于无人机旋翼产生的下洗气流对雾滴沉积过程具有显著影响,极易造成药液的漂移。为了研究旋翼下洗气流的流动特性和分布规律,本文提出了一种旋翼下洗气流速度分布的测试分析方法,设计了一种能够模拟六旋翼无人机不同旋翼转速状态下的旋翼旋转试验台,利用风速仪对旋翼不同径向位置产生的下洗气流进行了风速分布测量研究。研究表明旋翼径向各位置产生的下洗风速在旋转环线上分布较均匀,环向风速标准差小于 1m/s;沿旋翼径向各位置产生的下洗风速先增大后减小,1/2 旋翼半径处产生的下洗风速最大,试验中获得的最大下洗风速为 10.8m/s;旋翼产生的下洗风速随纵向变化不大,在距离地面 10cm 处受到地面效应的影响导致该高度下洗风速整体变小。通过以上研究结果可以得出旋翼径向各位置的翼型参数对该位置产生的下洗风速大小有显著影响,该研究成果为无人机旋翼下洗气流风速分布的研究提供了一种有效的测量方法,测量结果可为喷头在旋翼下方的分布及雾滴运动研究提供参考。

#### INTRODUCTION

In recent years, drones have been widely utilized in many fields, including agriculture (Xiongkui H. et al., 2017; Veroustraete. F, 2015) due to the popularity of civilian-grade drones.

Utilizing drones with pesticide spraying systems for crops such as rice, corn, cotton and tea, can effectively avoid the limitation of special field conditions and the state of crop growth on the plant protection machinery with large wheels (Xue X Y. et al., 2014), resulting in efficient, safe, and non-destructive plant protection. Numerous advanced technologies such as automatic path planning, unmanned operation and Real-time kinematic (RTK) high-accuracy positioning have been applied to multi-rotor drones (LU L, 2017; Wang Y. et al., 2018; Xu B et al., 2015) to considerably improve their operational stability, efficiency, accuracy and ease of operation. Consequently, multi-rotor drones have become the main models of plant protection drones in China. The most important feature of utilizing multi-rotor drones for pesticide spraying is

that it generates a powerful downwash during the flight due to its unique rotor structure and principle of motion, promoting the disturbance to crops and increasing the penetration of liquid. Therefore, liquid also has a good deposition effect on the lower part of crops (Yang Y S *et al.*, 2013, Reed W H, 1953).

However, due to the wide variety of drones that can be used for pesticide spraying, the specifications, numbers, and installation positions of various types of rotors differ. Therefore, large variations in downwash flow field are generated by different rotors. Thus, solving the problem of accurately depicting the overall spatial distribution characteristics of rotor downwash flow field and the distribution of downwash velocity at various locations inside the rotor is urgent.

Therefore, this study designs a test bed that simulates the rotor downwash flow field and measures and analyses the magnitude of the rotor downwash velocity and its distribution on the entire rotor through a uniform distribution point measurement method. This approach provides a basis for studying the spray performance of the nozzle in the downwash airflow field and the droplets settling. Moreover, improving the application effect of the multi-rotor plant protection drones is of considerable importance.

Scholars all over the world have conducted numerous studies to improve the application effect of agriculture drones. For example, Faical B.S. optimized the real-time flight path of the drone, which can independently adjust the flight route according to the changes in meteorological conditions (Faical B.S. *et al.*, 2017). However, changing the drone's flight route will also affect the deposition on the ground of droplets, which is not conducive to uniform spraying. Kirk studied the effects of boom length and droplet size on effective spray and spray drift, respectively (Kirk I.W. and Hoffmann W.C, 2002). Their results showed that the effective spray width produced when the boom length is 75% of the rotor diameter is less than the length of the boom equal to the diameter of the rotor. In addition, the droplet diameter of 400 microns has more drift compared with 1000 microns diameter of droplets to explore the effect of spray parameters on the deposition of wheat leaf in wheat disease prevention. However, the preceding studies did not reveal the influence of rotor airflow on the nozzles on different boom lengths. Fritz (Fritz B.K. *et al.*, 2006) conducted air spray tests to determine the type of spray head, particle size of spray droplets, and spray flow at the best deposition rate. However, environmental factors and the influence of the rotor airflow on the nozzle were not considered during the test; thus, the optimal parameters obtained were not universal.

The study of rotor downwash starts with helicopters. Quackenbush numerically calculated the flow field distribution of helicopter rotor/fuselage by applying the fuselage cell model and the free-wake method (Quackenbush T.R. *et al.*, 1994). Caradonna and Isom used a relatively simple potential flow equation to calculate the rotor flow without lift in the hovering state, but the application of the proposed method was limited for ignoring the lift (Caradonna F.X. and Isom M.P., 1972). Rajagopalan proposed a momentum source method for the simulation of helicopter flow fields in 1993 (Rajagopalan R.G. *et al.*, 1993). Wang Bo employed the momentum source method to investigate the numerical simulation of helicopter rotor and fuselage flow field and verified the effectiveness of the method (Wang B. *et al.*, 2008). Ren L.F. studied the influence of helicopter rotor field on the exhausted wake (Ren L.F. *et al.*, 2015). Sun Peng examined the influence of the outside wind on the helicopter rotor and the mixed airflow field on the deck (Sun P. *et al.*, 2015). Although these scholars mostly focused on aerodynamic characteristics of rotors and fuselage, the numerical simulations and tests extensively applied multi-rotor plant protection drones to crop pesticide spraying and achieved numerous research results (Xiongui H. *et al.*, 2017). The downwash airflow generated by the multi-rotor plant protection drone was studied to investigate its effect on the nozzle spraying characteristics and the deposition law of the droplets in the flow field. In response, Wang C.L. proposed a space mass balance test method (Wang C.L. *et al.*, 2016). The effects of 3WQF80-10 single-rotor plant protection drone on the mass balance distribution of the droplets in space and the distribution of the downwash velocity under the different flight modes and flight parameters analysed by outdoor experiments. Although the velocity of downwash generated by the rotors in different modes was measured, analysis of the causes of differences in droplet deposition due to the generated airflow fields with varying flight conditions is absent. Yang conducted a simulation experiment based on the XV-2 single-rotor agriculture drone to study the influence of downwash on the spray amplitude. The results showed that rotor downwash increased the spray amplitude (Yang Z.L. *et al.*, 2018). Tang utilized the high-velocity particle image velocity measurement method in the laboratory to obtain the movement of droplets under the rotor downwash (Tang Q. *et al.*, 2017). It was concluded that the downwash generated by rotors was the main factor affecting the droplet volume and sedimentation velocity. Yang adopted the CFD method to simulate the downwash air flow generated by the six-rotor drone and obtained the downwash velocity distribution rule of the rotor downwash at different height levels through a series of outdoor experiments (Fengbo Y. *et al.*, 2017).

Based on the preceding research literature, the downwash is found to have a considerable influence on the droplet sedimentation process and deposition effect. However, at present, scholars have studied the distribution of the overall downwash flow field generated by all rotors of a multi-rotor drone near the ground through different means. The differences in the downwash velocity distribution at varying positions inside the downwash flow field generated by each rotor due to the differences in rotor airfoil structure are neglected. This will directly affect the initial spray characteristics of the inner sprayer in the airflow field below the rotor. Therefore, a rotor rotation test bench is designed to measure and analyse the velocity distribution at different positions inside the downwash flow field generated during the rotation of any rotor.

The layout of this study is as follows. In Section 3, the structure and working principle of the rotor rotation test bench are introduced. In Section 4, the specific method of the velocity measurement test of rotor downwash airflow field is highlighted and the relative experimental results are analysed. In Section 5, the conclusions of this study are presented based on the experimental results.

## MATERIALS AND METHODS

### Structure and Principle of Test Bench

The frame of test bench is designed according to the six-rotor drone, with a wheelbase of 130 cm. In addition, the diameter of propeller is 56 cm. The frame is fixed on an aluminium profile support table that can be either raised or lowered (0-4m). The power part consists of brushless motor and electronic speed controller. The power source is the lithium battery (6s 18000mAH). The main structure is presented in fig.1.

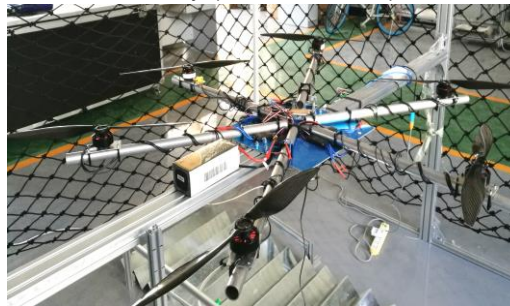


Fig.1 - The main structure of test bench

The control system and data acquisition system of test bench consist of computer, core controller and sensors. The core controller communicates with the computer through USB to TLL port line. With the use of the computer software, the rotation speed of rotor can be controlled remotely, and data, such as rotor tension, rotation speed, system voltage, current, throttle volume and throttle pulse width modulation (PWM) can be collected. The rotation speed measuring device is a photoelectric switch (QS18VN6D) produced by the Bonner Company. By attaching a black and white reflective paper on the wall of the motor, the photoelectric switch directly faces the motor wall to acquire the motor rotation speed signal, thereby obtaining the rotation speed of the rotor. The propeller pull can be measured by a pressure sensor (HX711AD) produced by the Gaoling company and located at the end of the rotor support. The downwash velocity of the rotor is measured by a wireless anemometer (410i) produced by Testo of Germany and data transmission is performed via Bluetooth. The parameters of each sensor are shown in table 1. And the control and data acquisition systems are presented in fig.2.

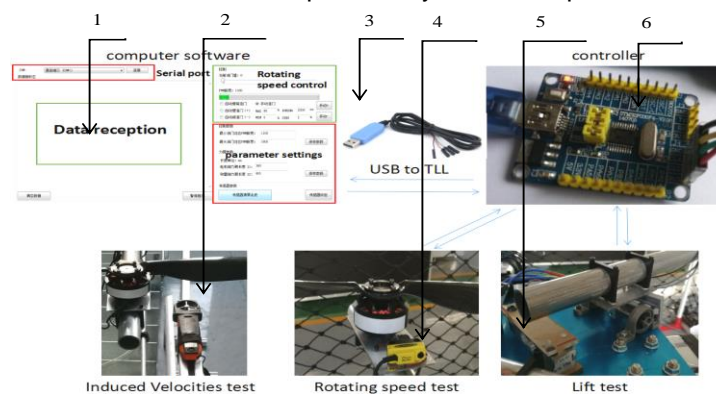


Fig.2 - The System of Control and Data Acquisition

1. Host computer interface 2. Anemometer 3. Serial cable 4. Photoelectric switch 5. Pressure sensor 6. Main controller

Table 1

Sensor Performance Parameters	
Range of tension sensor	Parameter value
Accuracy of tension sensor	0-10kg
Acquisition frequency of tensile sensor	1g
Range of velocity test	50hz
Frequency of velocity acquisition	0-10000r/min
Range of downwash velocity test	50hz
Accuracy of downwash velocity test	0.4-30M/s
Range of tension sensor	0.001m/s

**Downwash Velocity Measurement Test**

**Test Conditions**

The test is carried out in an airtight laboratory, the average temperature is 23°C indoor, the average humidity is 48%, the air density is 1.29 kg/m<sup>3</sup> and the air pressure is 1 standard atmosphere. To simulate the hovering state of the six-rotor drone under a take-off weight of 10 kg, the rotation speed can be maintained at 2500 r/min during the test.

**Measurement Point Arrangement**

The purpose of this test is to investigate the distribution law of downwash velocity of rotors in the horizontal cross-section and vertical cross-section of the downwash airflow. Thereby, the layout of the downwash velocity measurement points is as below:

(1) Horizontal Test Point Arrangement

To measure the velocity of the downwash generated at different radial positions of rotor blades, six measurement points (o, a, b, c, d, e) are set at the interval of 6 cm in the direction of the wing tip centring on the rotor rotation axis, and the radial measurement range is 0-30 cm. In the direction of the rotation of the blade, eight measuring points (N1-N8) are respectively arranged at the intervals of 45° on each equal-diameter ring so that the radial and circumferential directions of the blades together constitute the downwash-velocity measurement plane at the same height, for a total of 41 downwash velocity measurement points, as they are indicated in fig. 3(a).

(2) Vertical Test Point Arrangement

To investigate velocity of the downwash at different heights while the rotor is rotating, the rotating surface of the rotor is utilized as a reference plane, a total of 5 measurement planes (H1-H5) are set downward at a height interval of 20 cm and the range of vertical height is 0-100 cm. The layout scheme for each plane is the same as the horizontal layout scheme. The longitudinal distribution of the measurement points in the two directions of the same line is presented in fig. 3(b).

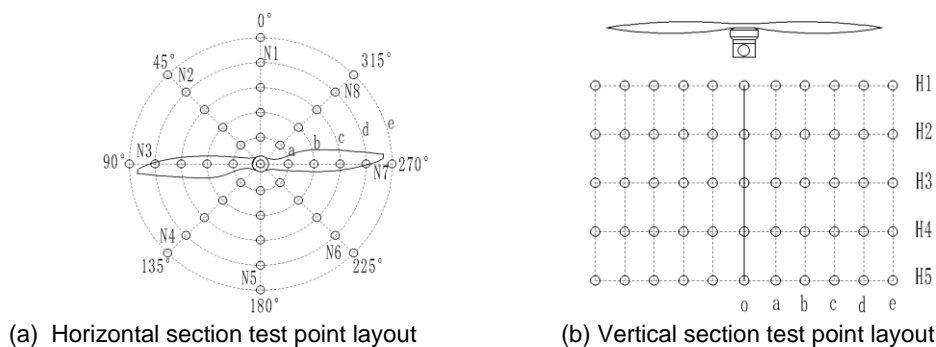


Fig. 3 - Below the rotor under the wash air velocity measurement point

**RESULTS**

**Downwash Velocity Results**

According to the layout scheme of fig. 3, the downwash velocity at each measurement point is measured. After the downwash is stable, the measured value of velocity can be recorded. Fig. 4 presents the average of the downwash velocity measurements at all the measurement points for each horizontal section height.

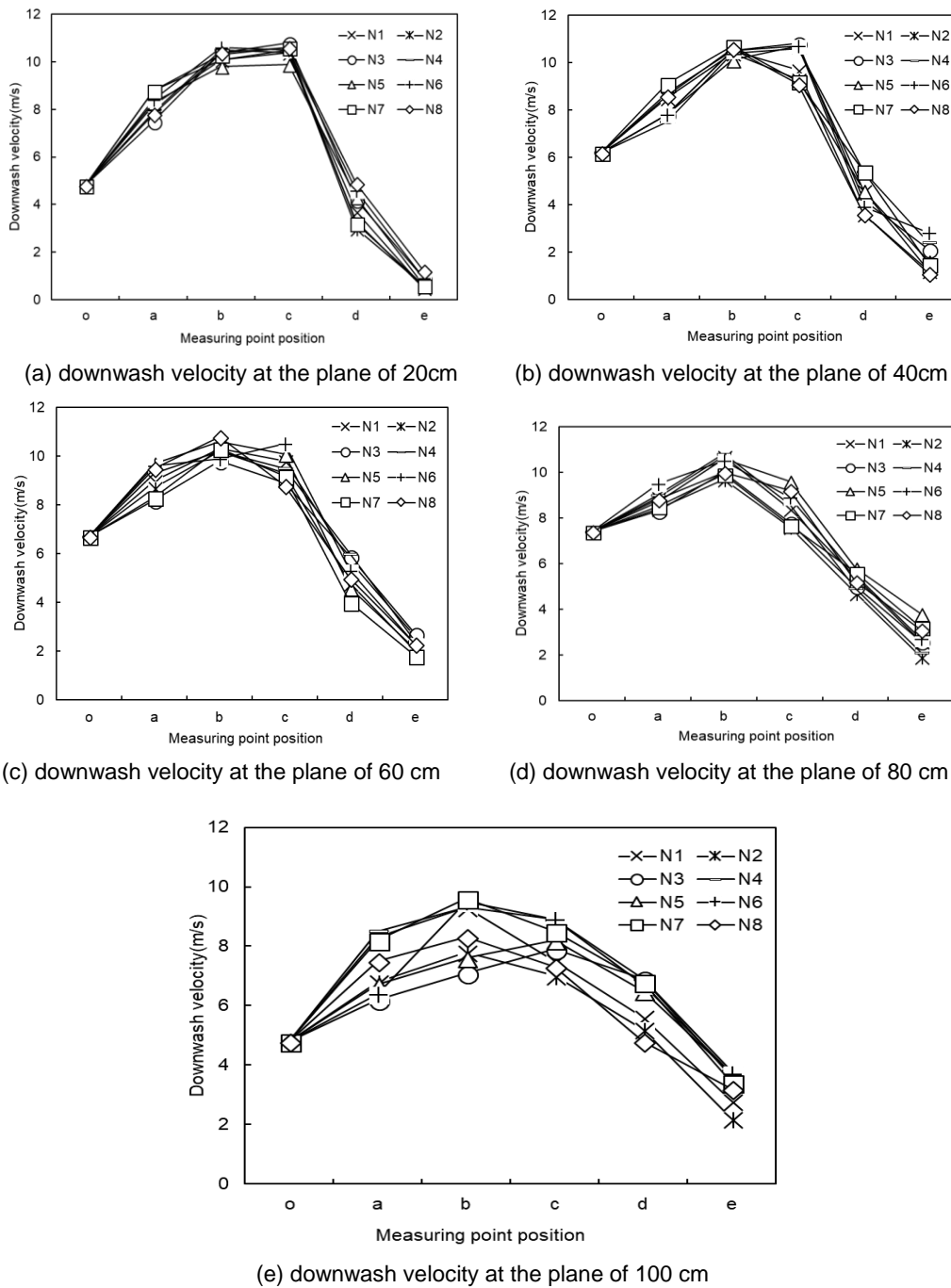


Fig.4 - The measurement results of rotor downwash velocity

**Standard Deviation Analysis of Downwash Velocity**

The standard deviation of the data reflects the degree of dispersion of a set of data and the average value. The deviation is calculated according to the following equation:

$$\sigma = \sqrt{\frac{1}{N} \sum_{i=1}^N (x_i - \mu)^2} \tag{1}$$

Where,  $\sigma$  is standard deviation, [m/s],  $N$  is the number of samples,  $x_i$  is the sample value, [m/s],  $\mu$  is sample mean.

This study calculates the standard deviations of eight measurements of downwash air velocity data for each radial position at each measurement height level, the results being presented in fig. 5.

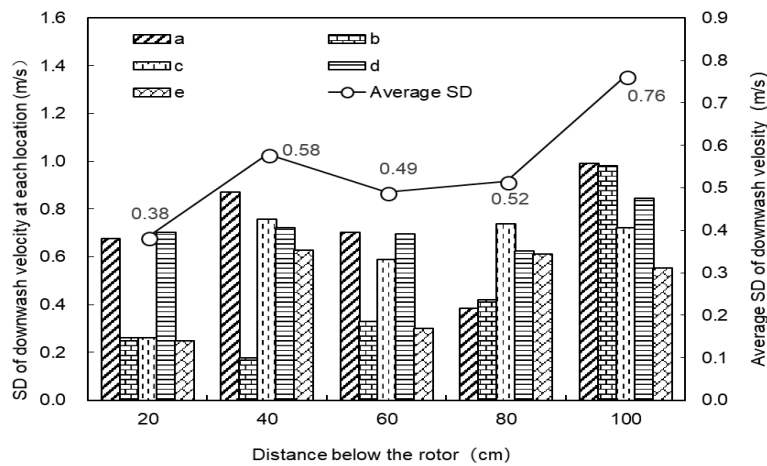


Fig. 5 - The Standard deviation of downwash velocity at each level below the rotor

The histogram in fig. 5 indicates the standard deviation of downwash velocity measurements in eight directions (N1 to N8) while five positions (a to e) rotate in five different height planes (H1 to H5).

In fig. 5 it can be seen that there are certain differences in the standard deviation of downwash velocity measurements at different positions in the same height and the differences in the rules are different at each height. The standard deviation of downwash velocity measurement results of the same radius position within the rotation circle is less than 1 m/s, which indicates that the downwash velocity generated at the same radius position of the rotation circle has no significant difference.

The discounted graph in fig. 5 presents the standard deviation of the average downwash velocity over the rotor radius at all the measurement locations as a function of the test height. It can be seen from the figure that with the increase of the test height, the standard deviation gradually increases, which suggests that the dispersion of the downwash velocity values at each measurement point increases. Nevertheless, the overall standard deviation is less than 1 m/s.

**Analysis of the Changing Law of Downwash Velocity**

The variation of the average downwash velocity generated by the rotor at each radial position with the radius is presented in fig. 6. The measured values of a~e in these six positions represent the downwash velocity of the downwash airflow generated while the rotor rotates at its centre position with the radius of 6 cm, 12 cm, 18 cm, 24 cm and 30 cm. Fig. 7 shows that the downwash velocity generated from the rotor centre position to the wingtip position suggests a changing trend of increasing first and decreasing later. The downwash velocity generated at the position of the rotor with the radius of 12 cm and 18 cm (b, c) is shown relatively close and is obviously higher than it was generated in other radial positions. The value of the downwash velocity generated at the tip of the rotor is the smallest. In the range of 20 cm-80 cm below the rotor, the variation of the downwash velocity produced by each radius position is basically the same and the change of the rules is slightly different at the height of 100 cm below the rotor due to the ground effect. Nevertheless, it conforms to the overall change trend.

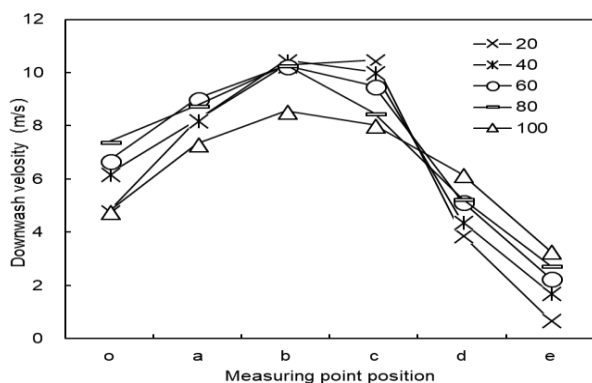


Fig. 6- Changes with the radial of downwash velocity

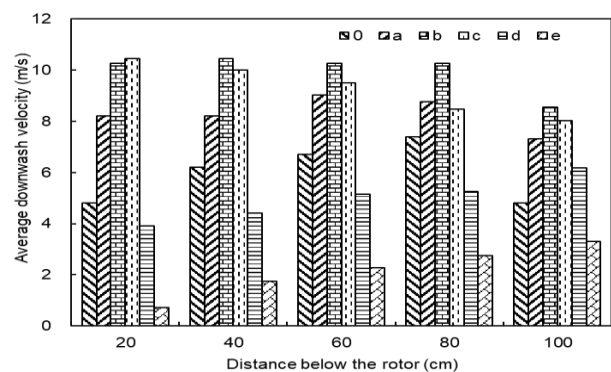


Fig. 7 - Changes with the height of downwash velocity

Fig. 7 presents the fact that downwash velocity varies with the height; it can be seen from the figure that the value of the downwash velocity generated at the centre of the rotor and the wing tip in the height range of 20-80 cm below the rotor increases with the height. The value of the downwash velocity generated at the rotor radius of 12 cm basically remains unchanged. The value of the downwash velocity generated at a rotor radius of 18 cm reduces with the height. Nevertheless, the variation of downwash velocity at 100 cm below the rotor is different from that of other positions since the position is closer to the ground and can be affected by the ground effect of the downwash airflow.

As it is shown in fig. 7, the average downwash velocity at the position of 'o' shows a trend of increasing first and decreasing later with the increasing height. This indicates that the downwash velocity generated by the inner rotor section is first compressed by the outer downwash airflow, leading to an increase in both airflow density and downwash velocity. Afterwards, due to the divergent lateral airflow, the density decreases, resulting in a decrease in downwash velocity. The average downwash velocity values at the positions of 'b' and 'c' decrease gradually with the increase of height, indicating that the downwash airflow generated in the middle of the rotor first compresses inward and then diverges outward, resulting in a decrease in the vertical airflow density at the position and leading to a decrease in downwash velocity. The downwash velocity generated at the positions of 'd' and 'e' increases with height, which suggests that the airflow generated by the rotor outer segment can be affected by the diffusion from the inside airflow, which strengthens the airflow density at this position as well as increases the downwash velocity. It can be inferred that the overall trend of the airflow field below the rotor is the convergence in the middle and the end diffusion, as presented in fig. 8.

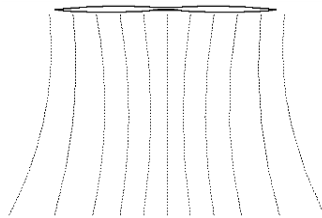


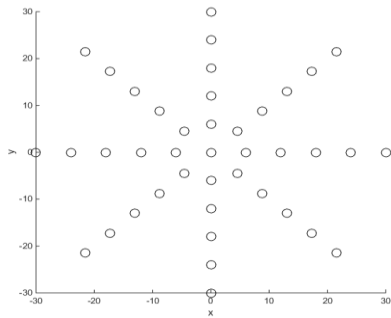
Fig. 8 - Trend of airflow field below the rotor

#### **Horizontal and Vertical Distribution of the Downwash Velocity**

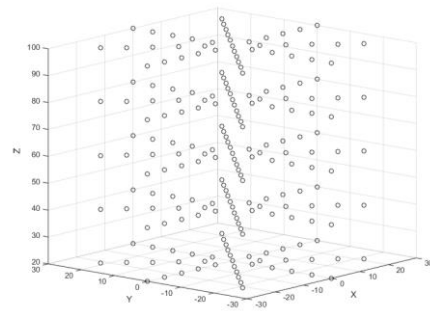
To investigate the distribution of downwash velocity in horizontal and vertical sections under the rotor, the central position of the rotor is utilized as the origin of coordinates to establish the plane coordinate system of downwash distribution at each height plane and the spatial coordinate system of downwash velocity distribution below the rotor. Besides, the corresponding coordinates of the measurement point and the space coordinates are calibrated. The distribution of the calibrated measurement points in the coordinates is presented in fig. 9. Fig. 9(a) shows the distribution of 41 measuring points in the plane coordinate system. Fig. 9(b) indicates the distribution of a total of 205 measuring points in spatial coordinate system. According to the data of the known measurement points, the downwash velocity distribution cloud diagram of the lower scrub flow at each height level can be plotted by interpolation with the usage of the Matlab software, as presented in fig. 10. It can be seen from fig. 10 that the downwash velocity generated by the lower scrubbing is higher than the one produced by other positions in the middle section of the rotor (10-20 cm). With the increase of altitude, the boundary of downwash velocity generated at each location is gradually blurred and the distribution of downwash velocity at the section becomes more uniformed.

All the collection points in the space can form vertical downwash velocity distribution planes in four directions of N1N5, N2N6, N3N7 and N4N8 according to fig.3. The interpolation method is utilized to complement the downwash velocity outside the measurement plane in the measurement plane, and the downwash velocity distribution cloud diagram is plotted with the usage of the Matlab software, as shown in fig.11. According to the vertical cross-section downwash velocity distribution cloud diagram of the downwash airflow field as shown in fig.11, the downwash airflow presents a diffusion trend from top to bottom, being consistent with the predicted trend in fig. 8.

The downwash airflow generated in the middle of the rotor has the largest downwash velocity below the rotor. At the near-ground end, the downwash velocity weakens due to the influence of the airflow field ground effect. According to fig. 11, the overall trend of the airflow fields distribution within the cross section of each value is the same, which also corresponds to the results of the standard deviation analysis of fig.5.

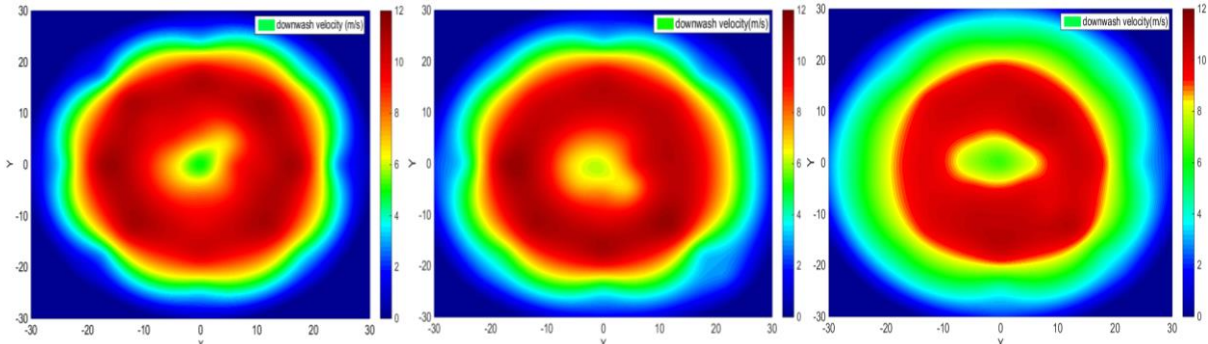


(a) Measurement point of plane calibration



(b) Measurement point of space calibration

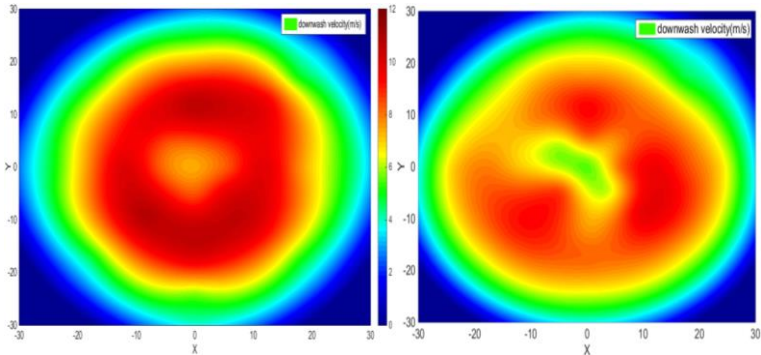
Fig. 9 - Coordinate calibration of measuring points



(a) 20 cm below the rotor

(b) 40 cm below the rotor

(c) 60 cm below the rotor



(d) 80 cm below the rotor

(e) 100 cm below the rotor

Fig. 10 - The downwash velocity cloud of the horizontal cross-section

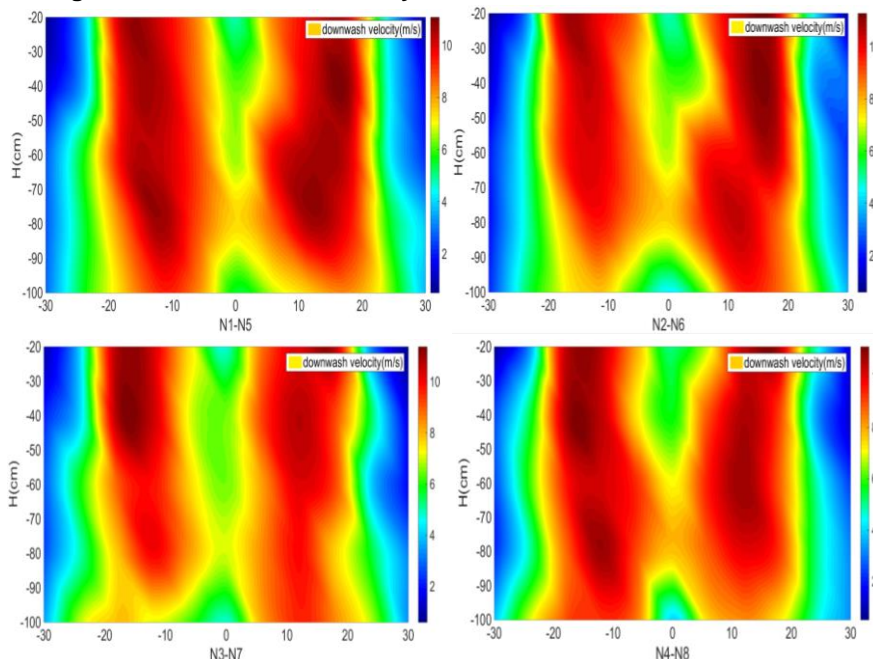


Fig. 11 - Distribution of downwash velocities in different vertical planes under the rotor

## CONCLUSIONS

To investigate the downwash velocity distribution of the downwash airflow generated by propellers of multirotor plant protection drone in the rotor diameter, this study designed a test bed for measuring the downwash velocity distribution of the rotor downwash airflow of the plant protection drone and adopted the multi-layer annular uniform distribution method. The downwash velocity distribution in the space below the rotor was measured and the results were analysed. Finally, the following conclusions were obtained:

(1) According to the standard deviation analysis of the airflow field data, at any height level below the rotor, the magnitude of the downwash velocity generated at the same radial position of the rotor has slight differences at each position on the rotation circle. The total standard deviation of data at each point of the wake increases with height but is less than 1 m/s in the range of 1 m below the rotor.

(2) From the centre to the tip of the rotor wing, the downwash velocity generated by each position is different. With the increase in radial distance, the downwash velocity increases first and decreases later. The maximum downwash velocity of 10.8 m/s can be measured on the 80 cm plane below the rotor.

(3) As the height increases below the rotor, the airflow gradually spreads to the surroundings and the area covered by the downwash gradually increases. Nevertheless, the magnitude of the downwash velocity in the high-speed region does not considerably change with the height. In this experiment, the effect of ground on the downwash velocity can be found at the height of 10 cm near the ground.

The results in this study can provide references for the arrangement of nozzles in the airflow field below the rotor and establish a foundation for the spatial motion trend analysis of the droplets in the rotor-downwash airflow field. Nonetheless, establishing an airflow field distribution model along the radial direction of the rotor and the height variation with the change of the rotor's own structural parameters is also necessary to clearly understand the changing law of the airflow under the rotor.

## ACKNOWLEDGEMENTS

The work was financially supported by National Key Technology Research and Development Program of the Ministry of Science and Technology of China (2014BAD06B01).

## REFERENCES

- [1] Bo W., Qi-jun Z., Guo-hua X., (2008), Numerical Simulation for the flow field of helicopter rotor/fuselage based upon Momentum-Source Method. *Helicopter technique*, Vol. 3, Issue. 06, Aviation Industry Corporation of China, Jingdezhen/China;
- [2] Caradonna F.X., Isom M. P., (1972), Subsonic and Transonic Potential Flow over Helicopter Rotor Blades. *AIAA Journal*, Vol. 10, Issue. 12, American Institute of Aeronautics and Astronautics, Reston/U.S.A., pp. 1606-1612;
- [3] Faical B.S., Freitas H., Gomes P.H., Mano L.Y., Pessin G., de Carvalho A.C., Ueyama J., (2017), An adaptive approach for UAV-based pesticide spraying in dynamic environments. *Computers and Electronics in Agriculture*, Vol. 138, Elsevier, New York/U.S.A., pp. 210-223;
- [4] Fengbo Y., Xinyu X., Ling Z., Zhu S., (2017), Numerical simulation and experimental verification on downwash air flow of six-rotor agricultural unmanned aerial vehicle in hover. *International Journal of Agricultural and Biological Engineering*, Vol. 10, Issue. 4, Editorial Office of IJABE, Beijing/China, pp. 41-53;
- [5] Fritz B.K, Kirk I.W., Hoffmann W.C., Martin D. E., Hofman V.L., Hollingsworth C., Halley S., (2006). Aerial application methods for increasing spray deposition on wheat heads. *Applied Engineering in Agriculture*, Vol. 22, Issue. 3, American Society of Agricultural and Biological Engineers, St Joseph/U.S.A., pp. 357-364;
- [6] Kirk I. W., Hoffmann W.C., (2002), Operational Factors Influence Spray Drift and Deposition from Helicopters. *ASAE Paper*, No. 02-AA06. American Society of Agricultural and Biological Engineers, St. Joseph/U.S.A.;
- [7] Lu., (2017), Application of BDS based on RTK in Agricultural Plant Protection Unmanned Helicopter. *Proceedings of the 8th China Satellite Navigation Academic Conference - S01 Satellite Navigation Application Technology*. Academic Communication Centre of China Satellite Navigation System Management Office. Shanghai/China;

- [8] Quackenbush T.R., Lam C. M. G, Bliss D. B., (1994), Vortex methods for the computational analysis of rotor/body interaction. *Journal of the American Helicopter Society*, Vol. 39, Issue. 4, American Helicopter Society, Alexandria/U.S.A., pp. 14-24;
- [9] Rajagopalan R. G., Mathur S. R. (1993), Three-dimensional analysis of a rotor in forward flight. *Journal of the American Helicopter Society*, Vol. 38, Issue. 3, American Helicopter Society, Alexandria/U.S.A., pp. 14-25;
- [10] Reed W. H. (1953), An analytical study of the effect of airplane wake on the lateral dispersion of aerial sprays. National Aeronautics and Space Administration, Washington DC/U.S.A.;
- [11] Ren L. F., Zhang J. Z., Shan Y., (2015), Effect of helicopter rotor downwash air flow on exhaust plume flow. *Journal of Aerospace Power*, Vol. 29, Issue. 1, Chinese Society of Aeronautics and Astronautics, Beijing/China, pp. 51–58;
- [12] Sun P., Geng X., Zhao X., Zhong J.J., (2015), Influence of wind directions on the flow field structures of helicopter rotor and deck. *Journal of Aerospace Power*, Vol. 30, Issue 08, Chinese Society of Aeronautics and Astronautics, Beijing/China, pp. 1802-1810;
- [13] Tang Qing, Zhang Ruirui, Chen Liping, Xu Min, Yi Tongchuan, Zhang Bin, (2017), Droplets movement and deposition of an eight-rotor agricultural UAV in downwash flow field. *International Journal of Agricultural and Biological Engineering*. Vol. 10, Issue. 3, Editorial Office of IJABE, Beijing/China, pp. 47-56;
- [14] Veroustraete F., (2015), The rise of the drones in agriculture. *EC agriculture*, E-Cronicon Journals, London /United Kingdom pp. 325–327;
- [15] Wang C., He X., Wang X., Wang Z., Wang S., Li L., Mei S., (2016), Distribution characteristics of pesticide application droplets deposition of unmanned aerial vehicle based on testing method of deposition quality balance. *Transactions of the Chinese Society of Agricultural Engineering*, Vol. 32, Issue. 24, Chinese Society of Agricultural Engineering, Beijing/China, pp. 89-97;
- [16] Wang Yu, Chen Haitao, Li Haichuan, (2018), A three-dimensional path planning method for plant protection UAV based on gravitational search algorithm. *Transactions of the Chinese Society of Agricultural Machinery*, Vol. 49, Issue. 02, Chinese Society for Agricultural Machinery, Beijing/China, pp. 28-33;
- [17] Xinyu X., Kang T., Weicai Q., Yubin L., Huihui Z., (2014). Drift and deposition of ultra-low altitude and low volume application in paddy field. *International Journal of Agricultural and Biological Engineering*, Vol. 7, Issue. 4, Editorial Office of IJABE, Beijing/China, pp. 23-28.
- [18] Xiongkui H., Bonds J., Herbst A., Langenakens J., (2017), Recent development of unmanned aerial vehicle for plant protection in East Asia. *International Journal of Agricultural and Biological Engineering*, Vol. 10, Issue. 3, Editorial Office of IJABE, Beijing/China, pp. 18-30;
- [19] Xu Bo, Chen Liping, Tan Hao, Xu Wei, (2015), Study on Minimum Energy Consumption Track Planning Algorithm for Multi-platform Operation Plant Protection UAV. *Transactions of the Chinese Society of Agricultural Machinery*, Vol. 46, Issue 11, Chinese Society for Agricultural Machinery, Beijing/China, pp. 36-42;
- [20] Yang Zhilun, Ge Luzhen, Zhai Lijun, Cheng Yifan, Wu Yalei, (2018), Study on the Effect of Rotor Washing Airflow on the Spray Rate of Plant Protection UAV[J]. *Transactions of the Chinese Society for Agricultural Machinery*, Vol. 49, Issue 01, Chinese Society for Agricultural Machinery, Beijing/China, pp. 116-122;
- [21] Yousheng Y., Jianping Z., Songlin N., (2013), Energy loss of nozzles in water jet system. *Journal of Mechanical Engineering*, Vol. 49, Issue 02, Chinese Mechanical Engineering Society, Beijing/China, pp. 139-145.